Fluctuating and sensory-induced vasodynamics in rodent cortex extend arteriole capacity

Patrick J. Drew[a,b,c], Andy Y. Shih[a], and David Kleinfeld[a,d,1]

[a]Departments of Physics and Neurobiology and [d]Center for Neural Circuits and Behavior, University of California, San Diego, CA 92093; and [b]Center for Neural Engineering and [c]Departments of Engineering Science and Mechanics and Neurosurgery, Pennsylvania State University, University Park, PA 16802

Edited* by Nikos K. Logothetis, Max Planck Institute for Biological Cybernetics, Tübingen, Germany, and approved March 28, 2011 (received for review January 10, 2011)

Neural activity in the brain is followed by localized changes in blood flow and volume. We address the relative change in volume for arteriole vs. venous blood within primary vibrissa cortex of awake, head-fixed mice. Two-photon laser-scanning microscopy was used to measure spontaneous and sensory evoked changes in flow and volume at the level of single vessels. We find that arterioles exhibit slow (<1 Hz) spontaneous increases in their diameter, as well as pronounced dilation in response to both punctate and prolonged stimulation of the contralateral vibrissae. In contrast, venules dilate only in response to prolonged stimulation. We conclude that stimulation that occurs on the time scale of natural stimuli leads to a net increase in the reservoir of arteriole blood. Thus, a "bagpipe" model that highlights arteriole dilation should augment the current "balloon" model of venous distension in the interpretation of fMRI images.

blood oxygen level-dependent functional MRI | neurovascular coupling | two-photon imaging | vasomotion | vibrissa somatosensation

Localized changes in the flow and volume of oxygenated blood in the brain are commonly used as a correlate of heightened neural activity. For two important imaging modalities, blood oxygen level-dependent functional magnetic resonance imaging (BOLD fMRI) (1) and intrinsic optical signal imaging (IOS) (2), the signals are generated by a complex interplay of the rate of oxidative metabolism, the flux of blood in the underlying angioarchitecture, and changes in vascular volume (3). The locus for the increase in vascular volume that follows sensory stimulation (i.e., arterioles or venules) is an enduring controversy that bears directly on interpreting and quantifying fMRI signals (4–6). To resolve this question, we used in vivo two-photon laser-scanning microscopy to image spontaneous and sensory evoked vascular dynamics in the vibrissa area of parietal cortex of awake, head-fixed mice. All data were collected through a reinforced thin-skull window (7) (Fig. 1*A*); this method obviates potential complications from inflammation or changes in cranial pressure that may occur with a craniotomy (8).

Results

Images of the pial surface and measurements of the diameter of the lumen of surface arterioles and venules were performed while the mouse sat passively (Fig. 1*B*). Dilations greater than 5% of the baseline diameter occurred with frequencies of 0.07 ± 0.05 Hz (mean ± SD, $n = 118$ arteries in six mice). The diameters of short segments of arterioles (red in Fig. 1*B*) exhibited relatively large spontaneous increases in the spectral range between 0.1 Hz and 1 Hz (Fig. 1 *C* and *D*). The peak amplitude of these fluctuations was 23% ± 10% of the initial vessel diameter across all arterioles, with instances of a 50% increases in diameter. Further, these low-frequency oscillations were strongly coherent and synchronous over a distance of several hundred micrometers across cortex (198 pairs of vessels, in six mice, that were separated by 20–315 μm; slope of coherence = 0.001 μm^{-1} [nonsignificant (NS)] and slope of phase shift = 0.0009 rad/μm (NS)) (red in Fig. 1*E*). In contrast, the coherence in fluctuations in diameter across midrange frequencies, defined as 1–3 Hz, was substantially reduced (red in Fig. 1*E*). Last, the slow spontaneous oscillations in arterial diameter seen in awake animals (Fig. 1*C* and Fig. S1) are greatly attenuated by urethane anesthesia (Fig. S2).

In contrast to the case for arteries, spontaneous changes in the diameter of surface venules are relatively small (Fig. 1 *B* and *C* and Fig. S2). The spectral content of these signals is similar to that seen for arterioles, although the amplitudes at low frequencies are substantially reduced (Fig. 1 *C* and *D*). Further, there was significant yet greatly reduced spatial coherence between pairs of venules (33 pairs of vessels), or even pairs of venules and arterioles (124 pairs of vessels), compared with pairs of arterioles in the 0.1- to 1-Hz range (Fig. 1*D*). The coherence at the midrange of frequencies remained low (Fig. 1*E*). We conclude that spontaneous fluctuations are relatively weak within the venous return from cortex, consistent with the dearth of contractile tissue in these vessels.

To examine the responses of cerebral vasculature to sensory stimuli, contralateral vibrissae were deflected with puffs of air; puffs aimed at the tail served as a control for general arousal (Fig. 2*A*). Repetitive stimulation for 30 s, similar to that used in fMRI experiments with anesthetized rodents (4) but much longer than the 0.5–2 s required for decision making in a vibrissa-based discrimination task with mice (9), caused a rapid and transient dilation of arterioles that was followed, on average, by a steadily increasing dilation (Fig. 2 *A*–*C*). The high variance of the latter dilation results in part from intermingled transient events (Fig. S3). The same stimulus caused only a slow distension in venules that was also substantially weaker than the distension in arterioles (Fig. 2 *B* and *C*); control puffs did not lead to sustained distension (Figs. S3 and S4). These changes do not result from a change in blood gases, which remained unchanged across the period of stimulation, with $pCO_2 = 31.1 \pm 1.7$ mm Hg; $pO_2 = 108 \pm 8$ mm Hg, and pH = 7.37 ± 0.01 (four animals). Shorter periods of stimulation accentuated the difference between arteriole and venuole responses. In particular, a single air puff led to a transient dilation of the arterioles, with a peak amplitude of 7.3% ± 6.5% of the initial vessel diameter, but produced no discernable venous dilation (Fig. 2*C* and Table 1).

The time constant for the rise and fall of the averaged change in dilation of individual arteriole diameters was 8 ± 8 s, whereas that for the change in the venous time constants was 44 ± 35 s (Fig. 2). After the termination of prolonged vibrissae stimulation, arteries constricted below their initial diameter (−2.2% ± 4.6% averaged 20–60 s after stimulus offset; $P < 0.005$). Urethane anesthesia greatly reduced the arterial response and completely blocked venous distension to sensory stimulation (Fig. S2 *C*–*F*). None-

Author contributions: P.J.D. and D.K. designed research; P.J.D. and A.Y.S. performed research; D.K. contributed new reagents/analytic tools; P.J.D. analyzed data; and P.J.D. and D.K. wrote the paper.

The authors declare no conflict of interest.

*This Direct Submission article had a prearranged editor.

[1]To whom correspondence should be addressed. E-mail: dk@physics.ucsd.edu.

This article contains supporting information online at www.pnas.org/lookup/suppl/doi:10.1073/pnas.1100428108/-/DCSupplemental.

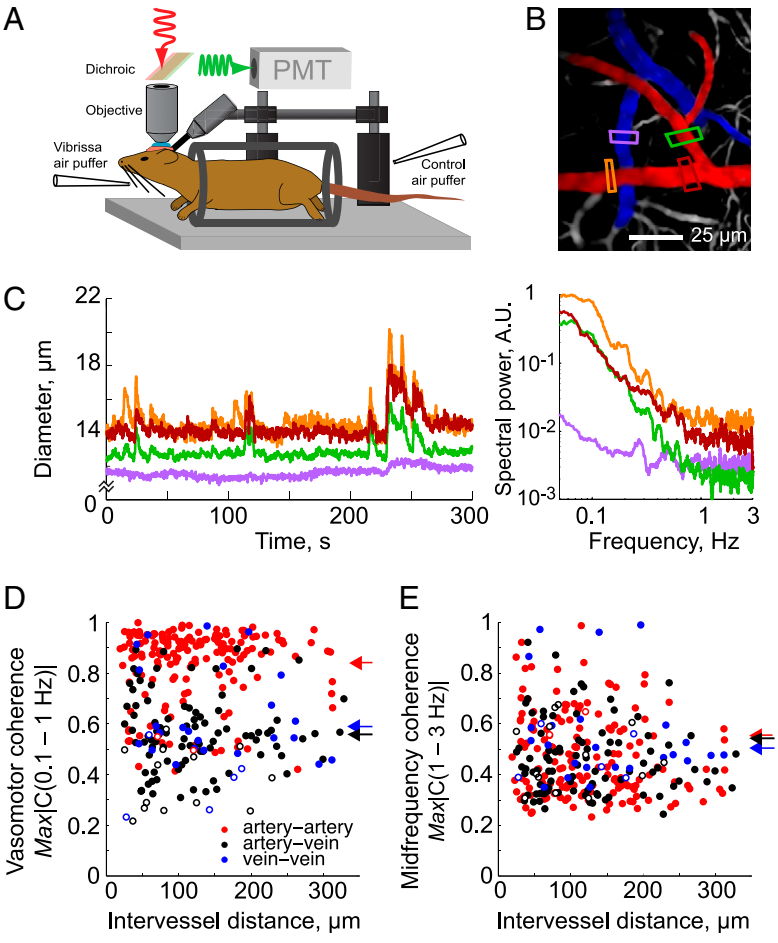

Fig. 1. Basic setup and spontaneous vascular dynamics in the cortex of awake mouse. (*A*) Schematic of the experimental setup. The awake mouse is head-fixed by means of a bolt and sits passively in an acrylic cylinder beneath the two-photon microscope. Air puffers for sensory stimulation are aimed at the vibrissa and as a control at the tail. (*B*) Example image of surface vessels. Arteries are highlighted in red, veins in blue. Colored boxes show regions where vessel diameter is measured. The intensity has been logarithmically compressed. (*C*) *Left:* Plot of vessel diameters of a quietly resting mouse from a representative 5-min span. *Right:* Power spectrum of the fluctuations in diameter of same vessels. Colors indicate the location of the segment of the vessel shown in *B*. (*D*) Plot of the maximal magnitude of the spectral coherence, |C(f)|, between pairs of vessels for 0.1- to 1-Hz band; bandwidth typically 0.1 Hz. Arteriole-to-arteriole |C| = 0.84 ± 0.15 (mean ± SD), 198 pairs (red). Venue-to-venule |C| = 0.58 ± 0.20, 33 pairs (blue). Arteriole-to-venule |C| = 0.55 ± 0.16, 124 pairs (black). Filled circles are for significant ($P < 0.01$; inverse of twice the number of degrees of freedom) values, hollow circles for nonsignificant values. Arrows on right indicate mean values across types of pairs. (*E*) Plot of the maximal magnitude of the spectral coherence between pairs of vessels for the 1- to 3-Hz band; 0.1 Hz bandwidth. Filled circles are for significant coherences, hollow circles for nonsignificant. Arteriole-to-arteriole |C| = 0.54 ± 0.10 (red). Venue-to-venule |C| = 0.51 ± 0.07 (blue). Arteriole-to-venule |C| = 0.54 ± 0.08 (black).

theless, the biphasic behavior seen in arterioles matched that observed after strong stimulation to anesthetized rodents (10).

The calculated blood volume changes in the arterial and venous compartments associated with different stimuli showed an approximately fourfold greater change in the arterial volume than in veins, as well as a slight poststimulus decrease in arterial blood volume (right-hand scale in Fig. 2*C*). Because the venous component of total blood volume is thought to be approximately three to four times that of the arterial component (6), the arterial volume changes dominate for brief stimuli and are likely to exceed the venous changes even for long stimuli. Finally, the diameter of subsurface capillaries (diameter = 2.9 ± 0.5 μm) was unchanged for all conditions of stimulation (Fig. S4), although capillaries with twice these diameters are reported to constrict in response to neuromodulation by central neurons in in vitro cerebellar and retina preparations (11).

Small arterioles dilated proportionally more than larger arterioles for both spontaneous dilation events and the rapid dilation that followed vibrissa simulation and vibrissae-evoked dilations (Fig. 3 *A* and *B*). In contrast, the delayed, second peak in the dilation does not show a significant dependence on vessel size (Fig. 3*B*), nor does the response to control stimuli (Fig. 3*C*). Under all conditions, venous distensions had no dependence on initial diameter. The dependence of spontaneous and evoked diameter changes on vessel size and type are similar to those observed under hypercapnia (6). The critical point is that both prompt and delayed arterial responses were similar in magnitude to spontaneous arterial dilations, with typical dilations of 30% and maximum dilations near 50% for both cases (Fig. 3 *A* and *B*).

We now ask whether the sensory evoked dilations of surface arterioles are reflected in the velocity of RBCs in the underlying capillaries (Fig. 4*A*). We find that a single puff of air to the vibrissae causes a transient increase in the speed of RBCs (Fig. 4 *B*–*D* and Table 2); systemic changes in blood pressure are unlikely to account for this effect because the increases in speed were not locked to changes in the heart rate triggered by the stimulus (Fig. S5). Further, stimulation for 30 s caused a transient increase in velocity, followed by a progressive increase that parallels the dilation in the surface arteries (Fig. 4*D*). These increases were not limited to the vibrissa area of parietal cortex, because vessels in the immediately adjacent medial region also respond to sensory stimuli (Fig. 4*C*). There was no significant difference in the relative increase in speed for vessels inside vs. outside the vibrissa area ($P > 0.32$, Kolmogorov–Smirnov test); the fraction increase in speed was 1.2 ± 0.1 ($n = 28$ vessels) within the vibrissa area, compared with an increase of 1.3 ± 0.2 ($n = 3$ vessels) outside the vibrissae area.

Discussion

Our results support a significant arterial contribution to a sensory-induced increase in blood volume, especially during the early portion of a sensory stimulation (Fig. 5). This is consistent with the overshoot of net-oxygenated blood, inferred from fMRI (6) and IOS (2) studies, that occurs after sensory stimulation. The expanded volume of arteriole blood leads to an increase in the velocity, but apparently not volume, of capillary blood. Constant capillary volume is consistent with a lack of capillary dilation even during epochs of seizure activity (12). For prolonged stimulation of the form typically used in fMRI experiments (4), but more than

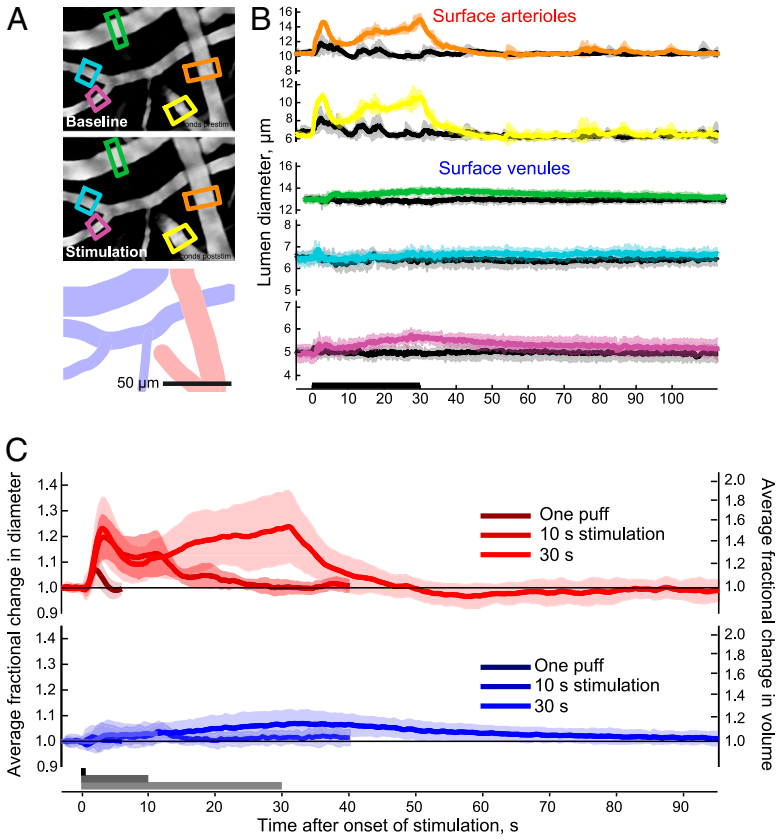

Fig. 2. Sensory evoked dilation of surface vessels. (*A*) Baseline image of vessels averaged 3–5 s before start of stimulation and the same vessels averaged 25–27 s after stimulus onset. Intensity has been logarithmically compressed. Illustration shows the location of veins and arteries in images. (*B*) Time course of the diameters of arterioles and venules in response to stimulation. Colored lines are in response to vibrissa stimulation, with the color indicating location of the diameter measurement in *A*; gray lines are control stimuli. Error bars indicate SD. (*C*) Normalized population volume changes (mean ± SD) for arterioles (*Upper*) and venules (*Lower*) for single puffs (28 arterioles and 7 veins), 10 s of puffs (17 arterioles and 8 venules), and 30 s of puffs (39 arterioles and 45 venules).

an order of magnitude longer than behavior time-scales, the continuous increase in flux eventually leads to an observable distension of the venules. In this case, the greater total volume of venous vs. arteriole vasculature (6) suggests that the increase in venous volume may be on parity with the increase in arteriole volume. The delayed increase in the volume of venous blood upon prolonged stimulation (Fig. 3), and the subsequent slow return of this volume to baseline levels, has been ascribed as evidence for "windkessel" (5) or "balloon" (4) models, in which the veins form a sink for excess blood. Rather, evolution has developed an arte-

Table 1. Stimulus-evoked vasodilation

	Punctate		10-s stimulus		30-s stimulus	
Parameter	Average (0.5–1.5 s after onset)	Peak	Average (0.5–10.5 s after onset)	Peak	Average (0.5–30.5 s after onset)	Peak
Surface arteries						
Vibrissa (%)	4.4 ± 4.5 ($P < 10^{-4}$)	8.9 ± 6.1 ($P < 10^{-5}$)	13.7 ± 7.0 ($P < 10^{-4}$)	22.0 ± 8.4 ($P < 10^{-5}$)	17.0 ± 9.6 ($P < 10^{-4}$)	25.8 ± 12.5; early* ($P < 10^{-5}$) 27.8 ± 10.7; delayed† ($P < 10^{-5}$)
Control (%)	1.9 ± 3.0 ($P < 3 \times 10^{-3}$)	5.0 ± 3.8 ($P < 10^{-5}$)	3.2 ± 3.3 ($P < 10^{-3}$)	9.6 ± 7.1 ($P < 10^{-5}$)	2.9 ± 4 ($P < 10^{-4}$)	12.1 ± 8.6; early* ($P < 10^{-5}$) 9.7 ± 8.4; delayed† ($P < 10^{-5}$)
Sample (*n*)	28		17		39	
Diameters (μm)	27.9 ± 13.7		16.5 ± 10.4		13.1 ± 7.5	
Surface veins						
Vibrissa (%)	−0.7 ± 0.8 (NS)	1.2 ± 1.2 (NS)	1.8 ± 3.5 (NS)	5.6 ± 3.3 ($P < 10^{-5}$)	4.1 ± 4.2 ($P < 10^{-4}$)	10.2 ± 6.2 ($P < 10^{-5}$)
Control (%)	−0.1 ± 0.1 (NS)	0.8 ± 0.9 (NS)	0.8 ± 1.4 (NS)	5.3 ± 4.1 ($P < 3 \times 10^{-3}$)	0.5 ± 3.3 (NS)	6.8 ± 5.7 ($P < 10^{-5}$)
Sample (*n*)	7		8		45	
Diameters (μm)	50.7 ± 23.7		17.0 ± 16.4		13.9 ± 8.3	
Capillaries						
Vibrissa (%)	−0.1 ± 3.0 (NS)				2.0 ± 5.1 (NS)	
Control (%)	−0.2 ± 1.7 (NS)				0.3 ± 2.5 (NS)	
Sample (*n*)	13				19	
Diameters (μm)	3.3 ± 0.6				2.9 ± 0.5	
Depth	30–50 μm below pia				20–50 μm below pia	

All numbers are mean ± SD.
*Early peak, which occurs in the 1- to 10-s period after stimulation.
†Delayed peak, which occurs 10–31 s after stimulation.

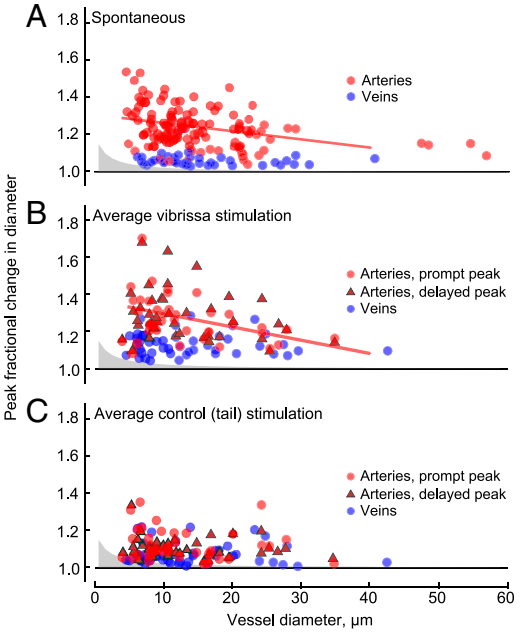

Fig. 3. Relationship between peak value of the dilation and vessel diameter. (*A*) Plot of peak spontaneous dilations for arteries, in red, and veins, in blue. Gray area shows the 0.2-μm resolution limit of detectable changes. The line shows the linear regression for arterioles, with a slope of $-0.004\ \mu m^{-1}$ (r^2 = 0.13, $P < 0.001$), whereas the slope for veins (not shown) is not significantly different from zero. (*B*) Plot of peak averaged dilation responses to 30-s vibrissae stimulation. Early arterial peaks, in the 0- to 10-s interval after stimulation, are denoted by red circles; regression slope = $0.007\ \mu m^{-1}$ (r^2 = 0.15, $P < 0.02$). Late arterial peaks, more than 10 s after onset, are denoted by red triangles; the linear regression (not shown) is not significant. Venuoles are denoted by blue dots; the linear regression is not significant. (*C*) Response to control stimulation. Note that spontaneous events had negligible contribution to the estimate of stimulus-induced events in *B* and *C*.

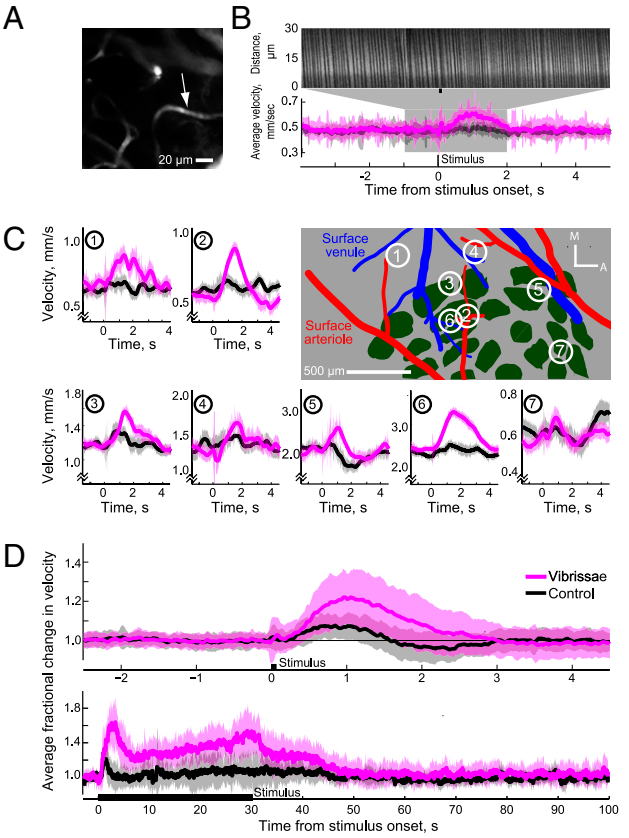

Fig. 4. Velocity increases caused by sensory stimulation. (*A*) Image of a capillary that lay 40 μm below the pial surface. (*B*) Velocity measurements from capillary in *A*. *Upper:* Raw line-scan data from a single trial showing increase in speed subsequent to vibrissa stimulation. *Lower:* Averaged velocity response to vibrissa (purple) and control (gray) stimuli. (*C*) Evoked increases in speed to single puffs, measured in and around the vibrissa-related area. Center shows histological reconstruction, green shows location of cytochrome-oxidase–rich regions that correspond to cortical columns, or "barrels," and large surface arterioles and venules are highlighted in red and blue, respectively. The symbols M and A refer to medial and anterior directions, respectively. (*D*) *Upper:* Plot of normalized population velocity response to a single air puff, effectively the "impulse response" (63 vessels). *Lower:* Plot of normalized population velocity responses during 30 s of stimulation (15 vessels).

rial "bagpipe" that serves as a reservoir of fresh blood to support the ongoing and anticipated increase in brain metabolic activity.

The BOLD fMRI signal is determined by an interplay of metabolism, blood flow, and vascular volume (13). Thus, the interpretation of the BOLD signal relies on understanding the changes in each of these components during functional hyperemia. The present optical-based results (Fig. 2) may be combined with MRI-based results (5, 14–17) to synthesize a view in which the relative contributions of changes on arterial and venous volumes depends upon the temporal characteristics of the stimulus. The rapid increase in blood flow to cortex that follows sensory stimulation, which occurs over a period of seconds, is accompanied by an increase in arterial cerebral blood volume. This causes an increase in oxygenation of the venous blood on the time scale of the arterial–venous transit time (16). If the stimulation is prolonged, ≈20 s or more in duration, a slow increase in venous blood volume gradually becomes a significant component of the blood volume change (14, 15). Under some conditions, capillary volume may also increase (18). In summary, transient sensory stimuli evoke substantial changes in the arteriole volume, whereas prolonged stimulation may lead to changes in volume throughout the entire vascular volume.

Our realization of two-photon microscopy (Fig. 1*A*) allows visualization of blood flow dynamics at the level of single vessels with transcranial illumination and detection in awake animals. However, it is currently limited to imaging the superficial aspects of the cortex, and even with extensive averaging we could not resolve changes in diameter less than 0.2 μm. Thus, changes in venous diameter of less than 2% and changes in capillary diameter of less than ≈7% would not be detected in our experiments but would contribute to total blood volume changes measured with MRI. Future work, using longer wavelengths (19) and adaptive optics (20–23) to correct for scattering by the thinned skull and brain tissue, should enhance the resolution and maximum depth of our images.

A final point concerns the low-frequency, coherent fluctuations in arterial volume that are seen in both the absence (Fig. 1*C*) and

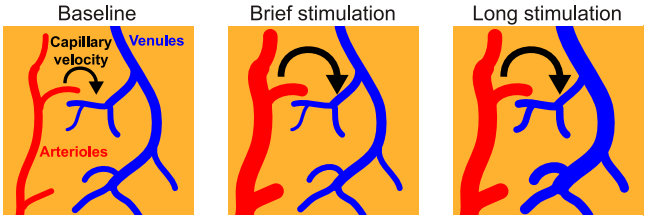

Fig. 5. Schematic summary of stimulus-induced changes in the cerebral vasculature. Brief stimulation leads only to arteriole distension, whereas a prolonged period of stimulation leads to an initial increase in arterial distension followed by a rise in capillary flow and finally venous distention.

Table 2. Stimulus-evoked increase in RBC velocity in capillaries

Parameter	Punctate stimulus (0.5–1.5 s after onset)	30-s stimulus (0.5–30.5 s after onset)
Vibrissa		
Mean (%)	20.6 ± 12.4 ($P < 10^{-4}$)	35.1 ± 15.1 ($P < 10^{-4}$)
Peak (%)	30.1 ± 14.6 ($P < 10^{-5}$)	81.8 ± 31.3 ($P < 10^{-5}$)
Control		
Mean (%)	7.9 ± 8.4 (NS)	5.1 ± 14.6 (NS)
Peak (%)	13.8 ± 6.0 (NS)	41.6 ± 38.6 ($P < 3 \times 10^{-2}$)
Sample	$n = 63$	$n = 16$
	Diameter = 4.9 ± 1.3 μm	Diameter = 3.2 ± 0.7 μm
	Depth range = 0–140 μm	Depth range = 20–50 μm

All numbers are mean ± SD.

presence of stimulation (Fig. 2*B*). The typical amplitude of the fluctuations can be larger than the average amplitude of the stimulus-initiated response. Thus, from the perspective of homeostatic regulation, changes in vascular diameter that occur in response to neuronal activation by external stimuli are comparable to spontaneous changes. Further, the frequency dependence and spatial coherence of oscillations seen here for surface arterioles is similar to that observed for slow spontaneous oscillations in the velocity of RBCs across capillaries (7). We conjecture that these result from vasomotion (24). The nature of these fluctuations seems similar to fluctuations in the BOLD fMRI signal in nonhuman (25) and human (26) primates and in the IOS and Doppler signals from rodents (24). Thus, the transcrianal imaging technique we used may be of use to explore the mechanistic basis of these ubiquitous oscillations (27) in behaving mice (28, 29).

Methods

Surgery and Experimental Procedures. All surgical and experimental procedures were performed in accordance with local Institutional Animal Care and Use Committee guidelines. Our subjects were 21 male c57/bl6 mice with masses greater than 20 g (Charles River). They were implanted with polished and reinforced thin-skull windows (7) over the vibrissa region of primary somatosensory cortex. A head-bolt was glued to the skull, and two or three self-tapping #000 screws (Small Parts) were threaded into the skull and attached to the head-bolt and skull via dental cement. Animals were allowed to recover for 2 d and then were acclimated to head fixation and vibrissa stimulation over 2–7 d. Imaging took place up to 4 mo after the initial surgery. Urethane (Sigma) anesthetized animals ($n = 2$) were injected with 1 g/kg urethane i.p. and 0.2 mg chlorprothixene (Sigma) i.m. (30). Additional animals for blood gas measurements ($n = 3$) were acclimated and had catheters inserted in their left femoral artery, as previously described (31), along with a head bolt.

Imaging and Data Analysis. Animals were imaged (32) using a custom two-photon microscope (33) that employed photon counting detection (34) and was controlled by MPScan software (35). We further used a 10× 0.3 N.A. (Zeiss), 20× 0.5 N.A. (Olympus), 20× 0.95 N.A. (Olympus), or 40× 0.8 N.A. (Olympus) dipping objective. Capillaries were imaged in the upper 200 μm of cortex. Power exiting the objective was typically 15–20 mW for imaging surface vessels and varied from 10 to 200 mW for capillaries. Baseline values of velocity and diameters exhibited no noticeable changes during 3–20 min of prolonged scanning.

Before each imaging session, animals were briefly anesthetized with isoflurane (2% in air) and infraorbitally injected with ≈0.05 mL 5% (wt/vol) 70 kDa fluorescein-conjugated dextran (Sigma) (36). Imaging sessions typically lasted 1 to 2 h. Sensory stimulation to the macrovibrissae of awake animals consisted of single 20-ms puffs of air (20 psi), delivered a distance of 3 cm from the vibrissae, either singly or in 8-Hz trains. This is known to cause a robust electrical response in the primary vibrissa area of the contralateral parietal cortex (37). Control stimuli were presented from an air puffer directed at the tail from 3 cm away. Stimuli were presented with 10- to 20-s interstimulus intervals for single puff stimuli, 60-s interstimulus interval for the 10-s stimulations, and 120-s interstimulus interval for the 30-s stimuli. Control and vibrissa stimuli were randomly interleaved.

For diameter measurements, movies were made from sequences of frames acquired at 6–30 frames per second. Individual frames were aligned to remove motion artifacts by calculating the maximum in the cross-correlation between the 2D Fourier transform of each image, yielding a phase shift that can be converted back to a translation in real space (38). Diameter measurements from frames that contained motion more than 4 μm over the entire field were excluded from further analysis. To determine the diameter of vessels from the movies, a small segment of the vessel, typically 2–5 μm, was manually selected and averaged along the long axis. The diameter was determined from the full width at half-maximum (39); we typically resolved changes down to 0.2 μm. For spontaneous measurements of diameter oscillations, only traces with more than 500 s of continuous data were used. Time series of the diameter were filtered with a three-point median filter, resampled at 25 Hz, and low-pass filtered with a 3-Hz first-order Butterworth filter for peak measurements. Multitaper coherence calculations (40, 41) and their error estimates (42, 43) were performed in MATLAB with the Chronux toolbox (44). Plots of spontaneous dilations were normalized by the median diameter. Those of sensory evoked changes in diameter were normalized to the value of the baseline diameter, defined as an averaged over the 2 s before stimulus onset. To estimate the time constant of the change in vessel diameter, the responses to 30-s stimuli were fit to boxcar functions convolved with an exponential (14); this yields equal rise and fall times.

For velocity measurements in the capillaries, line-scans were made of one or two vessels at a time with the use of arbitrary scan paths (45), from which velocities were calculated using the Radon transform method (46) implemented in MATLAB. Data were windowed into 40-ms windows with 10 ms of overlap. Exceptional points with separability score (46), a bootstrap measure of line-scan quality, of <3, or with a velocity that was less than one fourth or more than four times the mean velocity, were excluded from the averages. Velocity traces were filtered with a three-point median filter. Heart rate was determined from the peak in the power spectrum of the velocity within the 5- to 20-Hz band (7), obtained 0.5–1.5 s after the start of stimulation for the impulse or 0.5–30.5 s for the 30-s prolonged stimulation.

All statistics were performed with a two-sided *t* test, unless otherwise indicated, and all numbers are reported as mean ± SD. For peak velocities and diameters, the population maxima of the 1 s of baseline data were randomly resampled with replacement to match the duration that the maximum of the stimulus was measured over. A maximum of the resampled baseline data was taken and compared with the evoked response using a Kolmogorov–Smirnov test.

For histological reconstructions, animals were deeply anesthetized and transcardially perfused with PBS (Sigma), followed by 4% parformaldahyde (Sigma) in PBS followed by a 1% (wt/vol) fluorescein-albuminin (Sigma), 2% (wt/vol) gelatin (Sigma) mixture in PBS (47). The brain was extracted, the cortex flattened, fiduciary marks were made, and fluorescence images were taken to identify the locations of pial vessels relative to that of the fiduciary marks. After sinking in 20% (wt/vol) sucrose in PBS, we prepared 100-μm-thick brain sections tangential to the cortical surface and stained for cytochrome oxidase (48). The images of the vascular maps and cytochrome oxidase-stained sections were overlaid in Adobe Illustrator, according to the fiduciary marks, to determine the locations of imaged vessels relative to the cortical representation of the vibrissae (48).

Note Added in Proof. A recent paper has reported vasomotor oscillations in the intrinsic optical signal of mice (49).

ACKNOWLEDGMENTS. We thank the two anonymous reviewers for insightful comments; Richard Buxton for critical discussions with regard to stimulation parameters; Seong-Gi Kim and Tae Kim for discussions on models of the functional MRI signal and for graciously sharing unpublished data; Michael Fuentes and Carl Petersen for advice on head fixation; Jonathan Driscoll and Philbert Tsai for assistance with the imaging system; and Jonathan Driscoll and David Matthews for comments on an early version of the manuscript. This work was supported by National Institutes of Health Grants EB003832, MH085499, NS059832, and OD006831 (to D.K.) and by the American Heart Association (A.Y.S.).

1. Ogawa S, Lee TM, Nayak AS, Glynn P (1990) Oxygenation-sensitive contrast in magnetic resonance image of rodent brain at high magnetic fields. *Magn Reson Med* 14:68–78.
2. Grinvald A, Lieke EE, Frostig RD, Gilbert CD, Wiesel TN (1986) Functional architecture of cortex revealed by optical imaging of intrinsic signals. *Nature* 324:361–364.
3. Logothetis NK, Wandell BA (2004) Interpreting the BOLD signal. *Annu Rev Physiol* 66: 735–769.
4. Buxton RB, Wong EC, Frank LR (1998) Dynamics of blood flow and oxygenation changes during brain activation: the balloon model. *Magn Reson Med* 39:855–864.

5. Mandeville JB, et al. (1999) Evidence of a cerebrovascular postarteriole windkessel with delayed compliance. *J Cereb Blood Flow Metab* 19:679–689.
6. Lee SP, Duong TQ, Yang G, Iadecola C, Kim SG (2001) Relative changes of cerebral arterial and venous blood volumes during increased cerebral blood flow: Implications for BOLD fMRI. *Magn Reson Med* 45:791–800.
7. Drew PJ, et al. (2010) Chronic optical access through a polished and reinforced thinned skull. *Nat Methods* 7:981–984.
8. Sohler TP, Lothrop GN, Forbes HS (1941) The pial circulation of normal, non-anesthetized animals. Part 1. Description of a method of observation. *J Pharmacol Exp Ther* 71:325–330.
9. O'Connor DH, et al. (2010) Vibrissa-based object localization in head-fixed mice. *J Neurosci* 30:1947–1967.
10. Devor A, et al. (2007) Suppressed neuronal activity and concurrent arteriolar vasoconstriction may explain negative blood oxygenation level-dependent signal. *J Neurosci* 27:4452–4459.
11. Peppiatt CM, Howarth C, Mobbs P, Attwell D (2006) Bidirectional control of CNS capillary diameter by pericytes. *Nature* 443:700–704.
12. Fernández-Klett F, Offenhauser N, Dirnagl U, Priller J, Lindauer U (2010) Pericytes in capillaries are contractile in vivo, but arterioles mediate functional hyperemia in the mouse brain. *Proc Natl Acad Sci USA* 107:22290–22295.
13. Ogawa S, et al. (1992) Intrinsic signal changes accompanying sensory stimulation: Functional brain mapping with magnetic resonance imaging. *Proc Natl Acad Sci USA* 89:5951–5955.
14. Kim T, Kim SG (2010) Temporal dynamics and spatial specificity of aterial and venous blood volume changes during visual stimulation: Implication for BOLD quantification. *J Cereb Blood Flow Metab*, 10.1038/jcbfm.2010.226.
15. Kim T, Hendrich KS, Masamoto K, Kim SG (2007) Arterial versus total blood volume changes during neural activity-induced cerebral blood flow change: Implication for BOLD fMRI. *J Cereb Blood Flow Metab* 27:1235–1247.
16. Silva AC, Koretsky AP, Duyn JH (2007) Functional MRI impulse response for BOLD and CBV contrast in rat somatosensory cortex. *Magn Reson Med* 57:1110–1118.
17. Hirano Y, Stefanovic B, Silva AC (2011) Spatiotemporal evolution of the functional magnetic resonance imaging response to ultrashort stimuli. *J Neurosci* 31:1440–1447.
18. Stefanovic B, et al. (2008) Functional reactivity of cerebral capillaries. *J Cereb Blood Flow Metab* 28:961–972.
19. Kobat D, et al. (2009) Deep tissue multiphoton microscopy using longer wavelength excitation. *Opt Express* 17:13354–13364.
20. Ji N, Milkie DE, Betzig E (2010) Adaptive optics via pupil segmentation for high-resolution imaging in biological tissues. *Nat Methods* 7:141–147.
21. Rueckel M, Mack-Bucher JA, Denk W (2006) Adaptive wavefront correction in two-photon microscopy using coherence-gated wavefront sensing. *Proc Natl Acad Sci USA* 103:17137–17142.
22. Tsai PS, et al. (2007) Spherical aberration correction in nonlinear microscopy and optical ablation using a transparent deformable membrane. *Appl Phys Lett* 91: 191102.
23. Débarre D, et al. (2009) Image-based adaptive optics for two-photon microscopy. *Opt Lett* 34:2495–2497.
24. Mayhew JEW, et al. (1996) Cerebral vasomotion: A 0.1-Hz oscillation in reflected light imaging of neural activity. *Neuroimage* 4:183–193.
25. Vincent JL, et al. (2007) Intrinsic functional architecture in the anaesthetized monkey brain. *Nature* 447:83–86.
26. Biswal B, Yetkin FZ, Haughton VM, Hyde JS (1995) Functional connectivity in the motor cortex of resting human brain using echo-planar MRI. *Magn Reson Med* 34: 537–541.
27. Fox MD, Raichle ME (2007) Spontaneous fluctuations in brain activity observed with functional magnetic resonance imaging. *Nat Rev Neurosci* 8:700–711.
28. Komiyama T, et al. (2010) Learning-related fine-scale specificity imaged in motor cortex circuits of behaving mice. *Nature* 464:1182–1186.
29. Dombeck DA, Khabbaz AN, Collman F, Adelman TL, Tank DW (2007) Imaging large-scale neural activity with cellular resolution in awake, mobile mice. *Neuron* 56:43–57.
30. Kalatsky VA, Stryker MP (2003) New paradigm for optical imaging: Temporally encoded maps of intrinsic signal. *Neuron* 38:529–545.
31. Lee EJ, Woodske ME, Zou B, O'Donnell CP (2009) Dynamic arterial blood gas analysis in conscious, unrestrained C57BL/6J mice during exposure to intermittent hypoxia. *J Appl Physiol* 107:290–294.
32. Helmchen F, Kleinfeld D (2008) Chapter 10. In vivo measurements of blood flow and glial cell function with two-photon laser-scanning microscopy. *Methods Enzymol* 444: 231–254.
33. Tsai PS, Kleinfeld D (2009) In vivo two-photon laser scanning microscopy with concurrent plasma-mediated ablation: Principles and hardware realization. *Methods for Vivo Optical Imaging*, ed Frostig RD (CRC Press, Boca Raton, FL), 2nd Ed, pp 59–115.
34. Driscoll JD, et al. (2011) Photon counting, censor corrections, and lifetime imaging for improved detection in two-photon microscopy. *J Neurophysiol*, in press.
35. Nguyen QT, Tsai PS, Kleinfeld D (2006) MPScope: A versatile software suite for multiphoton microscopy. *J Neurosci Methods* 156:351–359.
36. Kleinfeld D, Mitra PP, Helmchen F, Denk W (1998) Fluctuations and stimulus-induced changes in blood flow observed in individual capillaries in layers 2 through 4 of rat neocortex. *Proc Natl Acad Sci USA* 95:15741–15746.
37. Drew PJ, Feldman DE (2007) Representation of moving wavefronts of whisker deflection in rat somatosensory cortex. *J Neurophysiol* 98:1566–1580.
38. Guizar-Sicairos M, Thurman ST, Fienup JR (2008) Efficient subpixel image registration algorithms. *Opt Lett* 33:156–158.
39. Shih AY, et al. (2009) Active dilation of penetrating arterioles restores red blood cell flux to penumbral neocortex after focal stroke. *J Cereb Blood Flow Metab* 29: 738–751.
40. Mitra PP, Ogawa S, Hu X, Uğurbil K (1997) The nature of spatiotemporal changes in cerebral hemodynamics as manifested in functional magnetic resonance imaging. *Magn Reson Med* 37:511–518.
41. Thomson DJ (1982) Spectral estimation and harmonic analysis. *Proc IEEE* 70: 1055–1096.
42. Kleinfeld D, Mitra PP (2011) Applications of spectral methods in functional brain imaging. *Imaging: A Laboratory Manual*, ed Yuste R (Cold Spring Harbor Lab Press, Cold Spring Harbor, NY), Vol 1, pp 12.11–12.17.
43. Fisher NI (1993) *Statistical Analysis of Circular Data* (Cambridge Press, Cambridge, MA).
44. Mitra PP, Bokil HS (2008) *Observed Brain Dynamics* (Oxford Univ Press, New York).
45. Valmianski I, et al. (2010) Automatic identification of fluorescently labeled brain cells for rapid functional imaging. *J Neurophysiol* 104:1803–1811.
46. Drew PJ, Blinder P, Cauwenberghs G, Shih AY, Kleinfeld D (2010) Rapid determination of particle velocity from space-time images using the Radon transform. *J Comput Neurosci* 29:5–11.
47. Tsai PS, et al. (2009) Correlations of neuronal and microvascular densities in murine cortex revealed by direct counting and colocalization of cell nuclei and microvessels. *J Neurosci* 18:14553–14570.
48. Drew PJ, Feldman DE (2009) Intrinsic signal imaging of deprivation-induced contraction of whisker representations in rat somatosensory cortex. *Cereb Cortex* 19: 331–348.
49. White BR, et al. (2011) Imaging of functional connectivity in the mouse brain. *PLoS One* 6:e16322.